Er and Gd Co-Doped Ceria-Based Electrolyte Materials for IT-SOFCs Prepared by the Cellulose-Templating Method

ALIYE ARABACI, VEDAT SARIBOĞA, and M.A. FARUK ÖKSÜZÖMER

$Ce_{0.9-x}Gd_{0.1}Er_xO_{1.9-x/2}$ ($0 \leq x \leq 0.1$) (EGDC) powders were successfully synthesized with a fast and facile cellulose-templating method for the first time and characterized by X-ray diffraction, scanning electron microscopy, and energy-dispersive X-ray spectroscopy. The samples were calcined at a relatively low calcination temperature of 773 K (500 °C). The sintering behavior of the calcined EGDC powders was also investigated at 1673 K (1400 °C) for 6 hours. Calcined $Ce_{0.9-x}Gd_{0.1}Er_xO_{1.9-x/2}$ ($0 \leq x \leq 0.1$) powders and sintered $Ce_{0.9-x}Gd_{0.1}Er_xO_{1.9-x/2}$ ($0 \leq x \leq 0.1$) pellets crystallized in the cubic fluorite structure. It was found that the relative densities of the sintered EGDC pellets were over 95 pct for all the Er contents studied. Moreover, the effect of Er content on the ionic conductivity of the gadolinium-doped ceria (GDC, $Ce_{0.9}Gd_{0.1}O_{1.90}$) was investigated. The highest ionic conductivity value was found to be 3.57×10^{-2} S cm^{-1} at 1073 K (800 °C) for the sintered $Ce_{0.82}Gd_{0.1}Er_{0.08}O_{1.91}$ at 1673 K (1400 °C) for 6 hours.

I. INTRODUCTION

SOLID oxide fuel cells (SOFCs) are the most efficient devices that convert the chemical energy of a fuel into electrical energy in a clean and cost-effective route. The cells have a high efficiency and large fuel flexibility at high temperatures. In general, conventional SOFC systems that use, the conventional SOFC electrolyte, yttria-stabilized zirconia (YSZ) as an electrolyte for their high conversion efficiency are operated at around 1273 K (1000 °C).[1,2] Operating at high temperatures 1273 K (1000 °C) has some difficulties such as interfacial reaction between the components, mechanical and thermal degradation, thermal expansion mismatch, and high cost materials. It is thus necessary to lower the operating temperature of the SOFCs. It is known that the replacement of YSZ electrolyte by the doped ceria which shows high ionic conductivity at low temperatures is one of the most promising methods for lowering the operating temperature.[3] The ionic conductivity of ceria increases significantly with the oxygen vacancies created by the doping of rare-earth cations into the ceria lattice. The ionic conductivity of doped ceria at 1023 K (750 °C) is similar to that of YSZ at 1273 K (1000 °C).[4] Among the various dopants used, Sm^{3+}, Dy^{3+}, and Gd^{3+} are favorable for increasing the ionic conductivity.[4,5] The literature reports show that GDC exhibits best of the high

ionic conductivity as SOFC electrolyte materials.[6,7] Furthermore, Kuharuangrong[4] reported that an increasing amount of Er from 10 to 20 mol pct reduces the conductivity of ceria and results in a separated phase of Er_2O_3 as detected by X-ray diffraction (XRD) and scanning electron microscopy (SEM). Therefore, in the present work, the maximum amount of Er was selected to be 10 mol pct. In addition, Jamshidijam et al.[8] studied the characterization of some selected rare-earth (RE)-doped ceria nanopowders such as $Ce_{0.9}Gd_{0.1}O_{1.95}$, $Ce_{0.9}Sm_{0.1}O_{1.95}$, $Ce_{0.9}Er_{0.1}O_{1.95}$, $Ce_{0.9}Pr_{0.1}O_{1.95}$, $Ce_{0.9}Nd_{0.1}O_{1.95}$, and $Ce_{0.9}Y_{0.1}O_{1.95}$ prepared via citric acid–nitrate combustion reaction.

It is well known that co-doping is an effective way for improving the conductivity of ceria-based electrolyte. In addition, to further improve the ionic conductivity, co-doped samples such as $Ce_{0.85}Gd_{0.1}Mg_{0.05}O_{1.9}$, $Ce_{1-a}Gd_{a-y}Sm_yO_{2-0.5a}$, $Ce_{0.8}Gd_{0.2-x}Pr_xO_{1.9}$, $Ce_{0.8}Sm_{0.2-x}Y_xO_{1.9}$, $Ce_{1-x-y}Sm_xLa_yO_{2-z}$, and $Ce_{0.8}La_{0.1}Y_{0.1}O_{1.9}$ have been studied.[9–14] However, to the best of our knowledge, there are no detailed studies in the literature about the $Ce_{0.9-x}Gd_{0.1}Er_xO_{1.95-x/2}$.

To obtain ceria-based electrolytes, various techniques have been used such as sol–gel,[15] hydrothermal synthesis,[16,17] homogenous precipitation[18,19], glycine–nitrate process,[20] combustion,[8,21] reverse microemulsion process,[22] and a variant of the sol–gel process known as cation complexation.[23]

Among the various chemical methods for preparing metal particles, the Cellulose-Templating method (CT) has been considered as a promising method to obtain metal oxide nanoparticles. The CT method is a simple technique to synthesize oxide-structured materials and is suitable for synthesizing the complex oxide powders with ultrafine size, high compositional homogeneity, and high purity, which is advantageous over the

ALIYE ARABACI, Assistant Professor, is with the Department of Metallurgical Engineering, Faculty of Engineering, Istanbul University, Avcilar, 34320 Istanbul, Turkey. Contact e-mail: aliye@istanbul.edu.tr VEDAT SARIBOĞA, Ph.D. Candidate, and M.A. FARUK ÖKSÜZÖMER, Associate Professor, are with the Department of Chemical Engineering, Faculty of Engineering, Istanbul University.

conventional solid-state method.[24] The CT method is used to synthesize oxide-structured materials in three steps: soaking of stoichiometric solution into a cellulose paper, drying, and calcination. Also drying step could be combined with combustion step. It was reported that mixed oxide structures which could be used as a SOFC component, were synthesized using CT method in literature.[25]

In this work, $Ce_{0.9-x}Gd_{0.1}Er_xO_{1.95-x/2}$ $(0 \leq x \leq 0.1)$ (EGDC) materials were synthesized by the simple and facile CT method for the first time. The crystallite sizes were determined by XRD analysis, and the sample densities were measured by Archimedes' method after sintering. The microstructural examinations and lattice parameter calculation of the Er and Gd co-doped ceria ceramics were performed. The ionic conductivity values of the samples were characterized using impedance spectroscopy measurements. This paper is intended to study the effect of Er addition on the structure and ionic conductivity of the gadolinium-doped ceria (GDC).

II. EXPERIMENTAL

A. Preparation of EGDC Powders and Pellets

The samples with the general formula of $Ce_{0.9-x}Gd_{0.1}Er_xO_{1.95-x/2}$ (where $x = 0.0$, 0.02, 0.04, 0.06, 0.08, 0.1) were synthesized by CT method as described elsewhere.[26] In this work, x was defined as the Er dopant amount which ranges from 0 to 0.10 mol pct. For example, 4EGDC sample refers to $Ce_{0.86}Gd_{0.1}Er_{0.04}O_{1.93}$.

Stoichiometric amounts of Ce $(NO_3)_3 \cdot 6H_2O$ (Sigma-Aldrich, 99.999 pct), Er $(NO_3)_3 \cdot 5H_2O$ (Sigma-Aldrich, 99.99 pct), and Gd $(NO_3)_3 \cdot 6H_2O$ (Sigma-Aldrich, 99.999 pct) salts were dissolved in de-ionized water, and 0.35 M[26] mixed salt stock solution was obtained according to the desired EGDC composition. At first, the solution was soaked into round ashless cellulose filter paper with 125-mm diameter and 0.2-mm thickness (pore sizes ≤2 μm, MACHEREY–NAGEL, MN 640 de) in the ratio of 1 mL solution per filter paper. Then, the solution-impregnated papers were put into a pre-heated furnace at 773 K (500 °C) without allowing the drying step in air. After all, the filter papers burned-out for 4 hours, the crispy residue was directly calcined at 773 K (500 °C). These directly calcined $Ce_{0.9-x}Gd_{0.1}Er_xO_{1.95-x/2}$, powders were ground in an agate mortar. Then, these ground powders were isostatically cold-pressed under 200 MPa (first, they were pressed with a pellet die in order to give the pellet shape under 0.5 MPa). Obtained pellets were sintered at 1673 K (1400 °C) for 6 hours. The flow chart of the CT method is given in Figure 1.

B. Characterization of the Samples

XRD technique was used to examine the crystalline structure. Calcined powders and the powders which were obtained by grinding the sintered pellets were studied by XRD using Rigaku D/max-2200 diffractometer with $CuK\alpha_1$ ($\lambda = 0.15406$ nm) radiation. The step scans were taken over the range of 2θ angles from
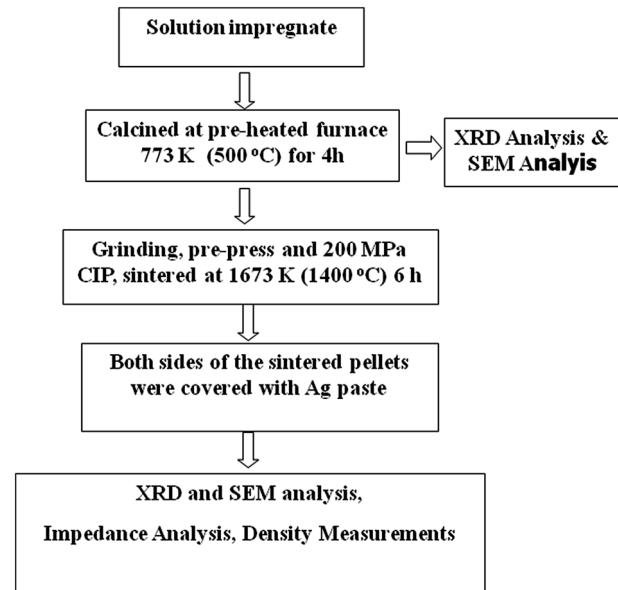

Fig. 1—Flow chart of CT method.

10 deg to 90 deg at a scanning rate of 2 deg min^{-1}. The average crystallite sizes (D) of the calcined samples were calculated using the well-known Scherrer method:

$$D = K\lambda / \beta \cos \Theta,$$

where K is the constant which was taken as 0.9, λ is wave length of the radiation (0.154 nm), β is the FWHM (full-width half maximum) of the (1 1 1) plane, and Θ is the diffraction angle (≈28.5 deg) of this plane.

The lattice parameter of the co-doped ceria was calculated from the peak position in the diffraction patterns according to Eq. [1]:[27,28]

$$a = d\sqrt{h^2 + k^2 + l^2}, \qquad [1]$$

where a is the cubic lattice parameter, d is the spacing between the planes in the atomic lattice, which is calculated by Bragg's law, and h, k, and l are the miller indices of the plane.

Microstructural and morphological features of the sintered pellets were investigated by SEM analysis. FEI-QUANTA FEG 450 scanning electron microscope was used to study the morphology and microstructure of the sintered samples. The elemental distribution of the sintered samples was also investigated by the Energy-dispersive X-ray spectroscopy (EDS), and the mapping images were obtained by scanning 32 frames.

The calcined powders were pressed with a cold isostatic press (CIP) at 200 MPa to obtain a disk-shaped test sample for the densification test. The compact disk samples were then sintered at 1673 K (1400 °C) for 6 hours. The densities of the sintered disks were determined by the well-known Archimedes' method. After determination of the bulk density, the relative density (RD) of the samples was obtained by dividing the bulk density to the theoretical density. Theoretical density of the samples was calculated using the lattice parameters obtained from the XRD analysis.

Impedance measurements were taken in a frequency range of 10 MHz to 10 mHz with a 20-mV perturbation using SOLARTRON 1260 FRA and 1296 interface, and Nyquist curves were plotted. For the measurements of ionic conductivity, initially, both sides of the sintered pellets were covered with Ag paste and fired at 1073 K (800 °C) for 30 minutes (firing). Then, the ionic conductivity measurements of the sintered pellets were taken within 50 K (50 °C) intervals in the temperature range of 473 K to 1073 K (200 °C to 800 °C) in air.

III. RESULT AND DISCUSSION

A. CT Method for the Preparation of EGDC

CT method consists of impregnation of salt solution into the pores of the cellulose filter paper. Figures 2(a) and (b) exhibit SEM images of a non-impregnated filter paper. As seen from Figure 2, the cellulose paper is compactly packed and has a low void volume. The metal salt solution containing gadolinium, cerium, and erbium nitrate was impregnated into the pores of the filter paper and then burned-out at 773 K (500 °C). The mixture of decomposed salt species was entrapped in the free domains of the filter paper. As seen in Figure 2(d), after the removal of the cellulose paper, networked fiber structure of Er-Gd-Ce-O mixture which consists of mesh-like regions was obtained. During the calcination process, only the solid-state reaction proceeded between the constituents due to the complete removal of the cellulose paper, and thus, this technique is named as ''improved solid-state reaction.''[29]

The phase evolution of the precursors after calcination was determined using XRD. The XRD patterns of the $Ce_{0.9-x}Gd_{0.1}Er_xO_{1.9-x/2}$ powders are shown in Figure 3. According to the XRD results, crystallization of the powders occurred at 773 K (500 °C). These results indicate that the products consist of single phase $Gd_{0.1}Ce_{0.9}O_{1.95}$ with a cubic fluorite structure (JCPDS Card No: 75-0161). No peaks were detected for the gadolinium oxide or erbium oxide. The results show that the dopant ion was fully substituted in the CeO_2 lattice.

The crystallite sizes of the calcined $Ce_{0.9-x}Gd_{0.1}Er_xO_{1.9-x/2}$ samples were around 10.6 nm. This value is compatible with the other studies done by different synthesizing methods[8,30,31] which are more complex than CT method. It is well known that lower crystallite sizes enable the production of ceramics with higher densities.[32]

The sintered $Ce_{0.9-x}Gd_{0.1}Er_xO_{1.9-x/2}$ pellets crystallized in the cubic fluorite structure are shown in Figure 4. The reflection peaks for sintered powders became sharper and narrower than those of the calcined powders. This indicates that the sintering process leads to an increased crystallite size (between 30 and 40 nm)
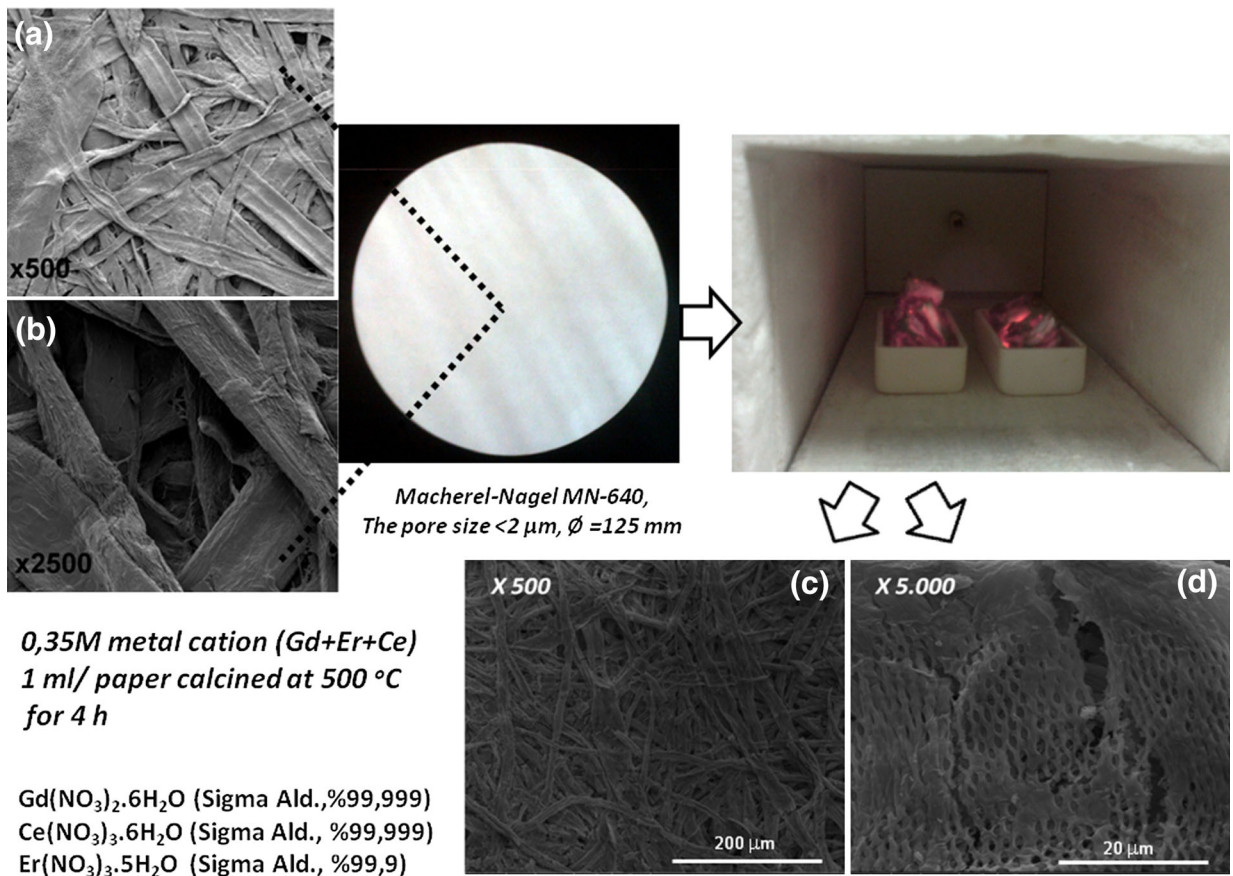

0,35M metal cation (Gd+Er+Ce)
1 ml/ paper calcined at 500 °C
for 4 h

$Gd(NO_3)_2.6H_2O$ (Sigma Ald.,%99,999)
$Ce(NO_3)_3.6H_2O$ (Sigma Ald., %99,999)
$Er(NO_3)_3.5H_2O$ (Sigma Ald., %99,9)

Fig. 2—SEM images of (a) non-impregnated filter paper for (×500), (b) non-impregnated filter paper for (×2500), (c) impregnated and burned-out filter paper (×500), and (d) impregnated and burned-out filter paper (×5000).
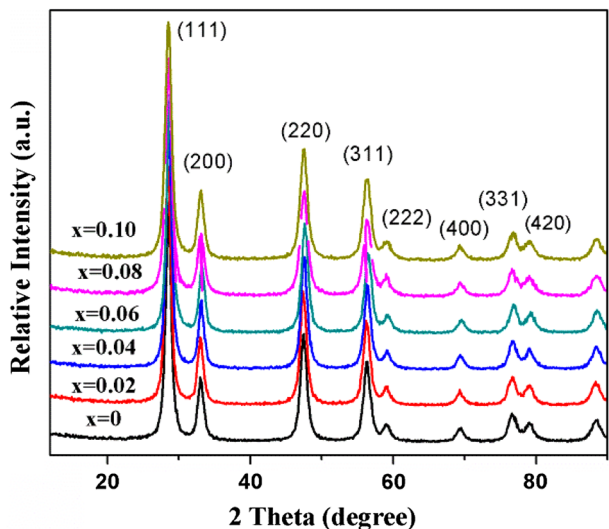
Fig. 3—XRD patterns of the calcined at 773 K (500 °C) $Ce_{0.9-x}Gd_{0.1}Er_xO_{1.9-x/2}$ powders.

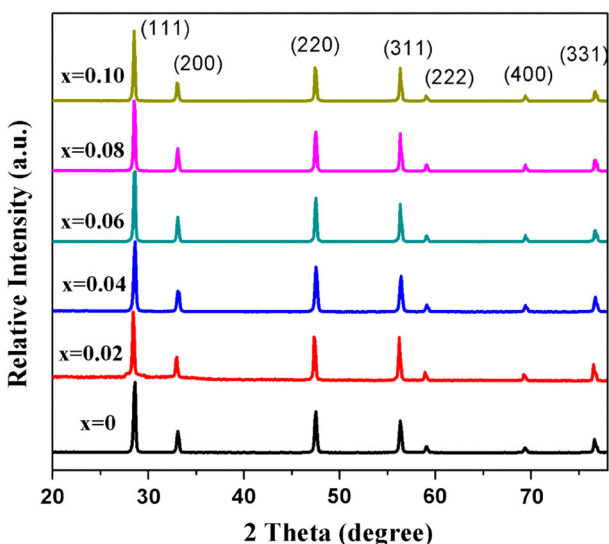Fig. 4—XRD patterns of GDC with different Er contents sintered at 1673 K (1400 °C).

Fig. 5—Measured lattice parameters of Er pct doped GDC10 solid solutions as a function of dopant concentration.

and improved crystallinity. After sintering at 1673 K (1400 °C), the calculated lattice parameters of the samples are 5.418 Å for 0 mol pct Er-doped GDC and 5.405 Å for 10 mol pct Er-doped GDC, which indicate solid solution formation, because the lattice parameter of pure ceria is 5.411 Å.[33]

The measured lattice parameters are plotted in Figure 5 as a function of x. As can be seen from Figure 5, the lattice parameter linearly decreases with the increasing Er content in the range of x = 0 to 0.10, although the ionic radius decreases in the order of Gd^{3+} (0.1053 nm) > Er^{3+} (0.1004 nm) > Ce^{4+} (0.097 nm)]. Hong and Virkar[34] measured lattice parameters of various RE oxide-doped ceria solid solutions as a function of dopant concentration, and they reported that when the La, Nd, Sm, and Gd are used as dopants,
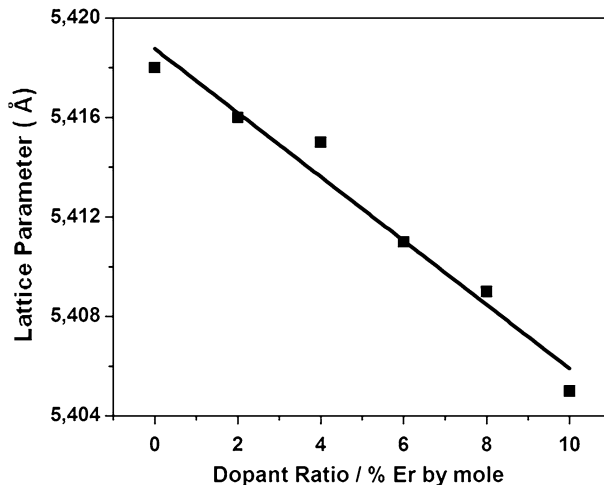
the lattice parameter of ceria increases. On the other hand, the lattice parameter decreases with the addition of Er, Dy, Ho, and Yb. Similar results were also found in our research.

B. Density Measurements and SEM Analysis

Figure 6 shows the SEM images of the calcined Er-doped GDC sample for 4 hours. Figure 6(a) exhibits that fibers were long, elongated, and thin. It is clear that all fibers were homogeneous, and even the fibers underneath the surface have the same structure. Mesh-like structure is observed in Figure 6(b). The porous morphologies of the calcined EGDC samples are likely to be caused by large volumes of gas produced in the paper burn-out process. During the combustion process, a large amount of gaseous material was evolved, and hence, the combustion product is highly porous as shown in the SEM micrographs (Figures 6(a) through (c)).

Figure 7 shows SEM micrographs of the EGDC samples, sintered at 1673 K (1400°C) for 6 hours. All the sintered samples were composed of nearly fully dense structure and had uniform structure. A significant change was not observed on the grain size of GDC with the increasing Er amount (Figure 7). All samples have 0.1 to 1 μm average grain size. The densities of all the sintered pellets had the same RD values which were above 95 pct. This value is comparatively higher than the values of the previously reported results.[35,36]

The EDS analysis results of the samples are given in Figure 8. As can be seen, the surface composition of the samples is very close to the desired stoichiometry. A randomly selected area shows the target composition for the all samples. When SEM images of the samples were investigated in detail, many small, homogeneously distributed particles are seen over the grains. This figure created suspicion that if the small particles between the regular grains were due to Er_2O_3 or Gd_2O_3 not incorporated into CeO_2 lattice. To overcome the suspicion, SEM–EDS map analyses were performed on the outer
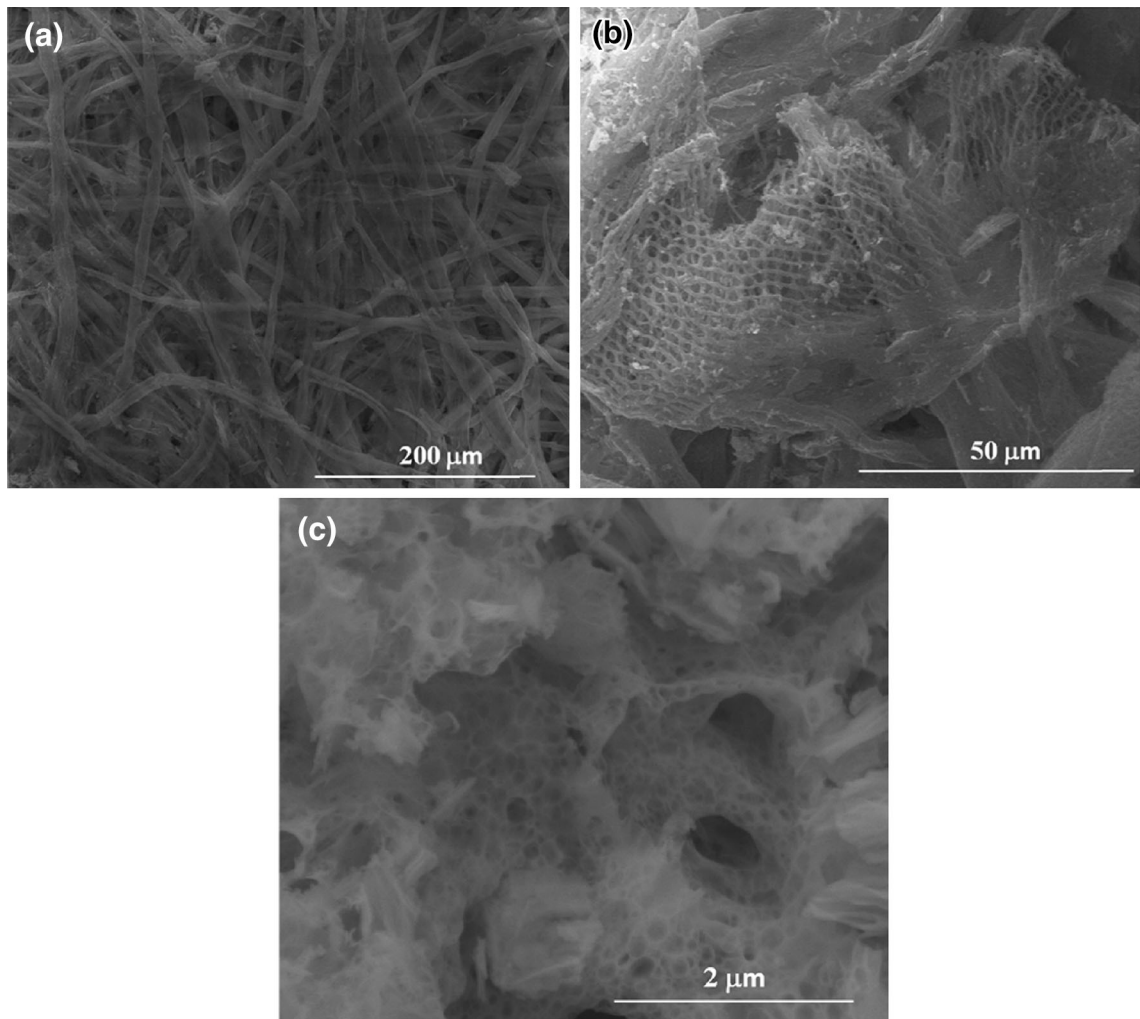
Fig. 6—SEM images of impregnated and burned-out filter paper obtained at magnifications of (*a*) (×500), (*b*) (×2500), and (*c*) (×50,000).

surface of 2EGDC sample which is given in Figure 9. This figure shows that the small particles do not belong to Er or Gd species. Ce, Gd, and Er are uniformly dispersed in the structure. The small particles are highly possible related with the insufficient sintering of the tiny particles of the sample.

C. *Electrochemical Impedance Spectroscopy Analysis*

Electrochemical Impedance Spectroscopy (EIS) uses electronically conducting electrodes to characterize the electrical properties of the materials and their interfaces. The evaluation of the electrochemical behavior of the electrolyte and/or electrode materials is carried out by applying voltage to electrodes and observing the response.[37] Bauerle[38] introduced for the first time the use of impedance spectroscopy to determine the oxygen ionic conductivity. SOFC electrolytes are oxygen ion conductors; therefore, they can be studied using this technique. Impedance spectroscopy is an important technique to investigate the mobile charges in ionic, semi-conducting, or insulating solids. Moreover, this characterization method can be also used to measure the

resistance, or the impedance of the grain boundary, the grain, and the electrode of a sample.[39]

In the existing studies in the literature, it is reported that the ionic conductivity of the electrolyte material enhanced when ceria was doped with trivalent RE elements. Especially 10 mol pct Gd-doped ceria was pointed out be the best.[36,40,41] In order to further improve the ionic conductivity of GDC with this composition, co-doped or double-doped studies have been carried out by many researchers and most of them acquired positive results.[42–44] For example, Gd and Sm co-doped ceria gave higher conductivity than each single-doped ceria.[43,44] However, more studies to optimize the dopants type and to understand how they affect the ionic properties are required. Depending on this situation, co-doped ceria materials using Er as dopant were synthesized, and the effect of Er addition on the structure and ionic conductivity of the GDC was investigated.

The ionic conductivity measurement was performed in air atmosphere in the temperature range of 473 to 1073 K (200 °C to 800 °C). A complex plane plot of real impedance, Z', *vs* imaginary impedance, Z'', was
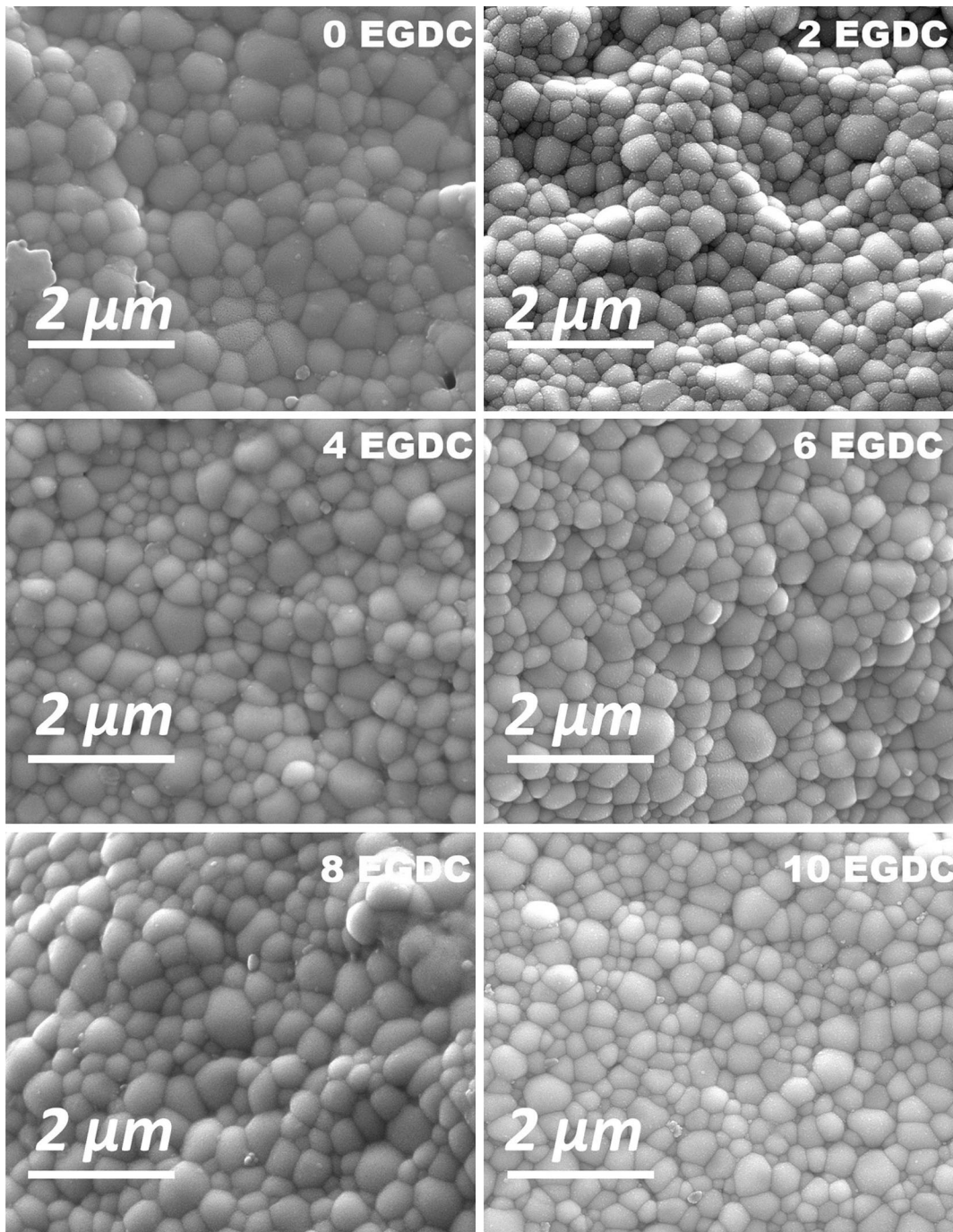
Fig. 7—SEM images of the EGDC sample surfaces.

prepared for each set of data. By curve fitting a circle to semicircles on these plots, sample resistances (R) were obtained. The total conductivity (σ_T) values were then calculated from the total resistance (R_{total}), cross-sectional area (A), and thickness (l) by using the following equation:

$$\sigma_T = \frac{l}{A \cdot R_{total}}. \qquad [2]$$

Figure 10(a) presents the complex impedance spectra of EGDC samples measured in air at 573 K and 1073 K (300 °C and 800 °C). Figures 10(a) and (b) show low temperature [573 K (300 °C)] EIS results and (c) is for high temperature [1073 K (800 °C)]. The ionic conductivity of the materials shows conductivity with the order 8EGDC ($Ce_{0.82}Gd_{0.1}Er_{0.08}O_{1.91}$) $\approx$ 2EGDC > GDC > 10EGDC > 4EGDC > 6EGDC. As can be seen in Figure 10(a), addition of Er lowered the ionic resistance
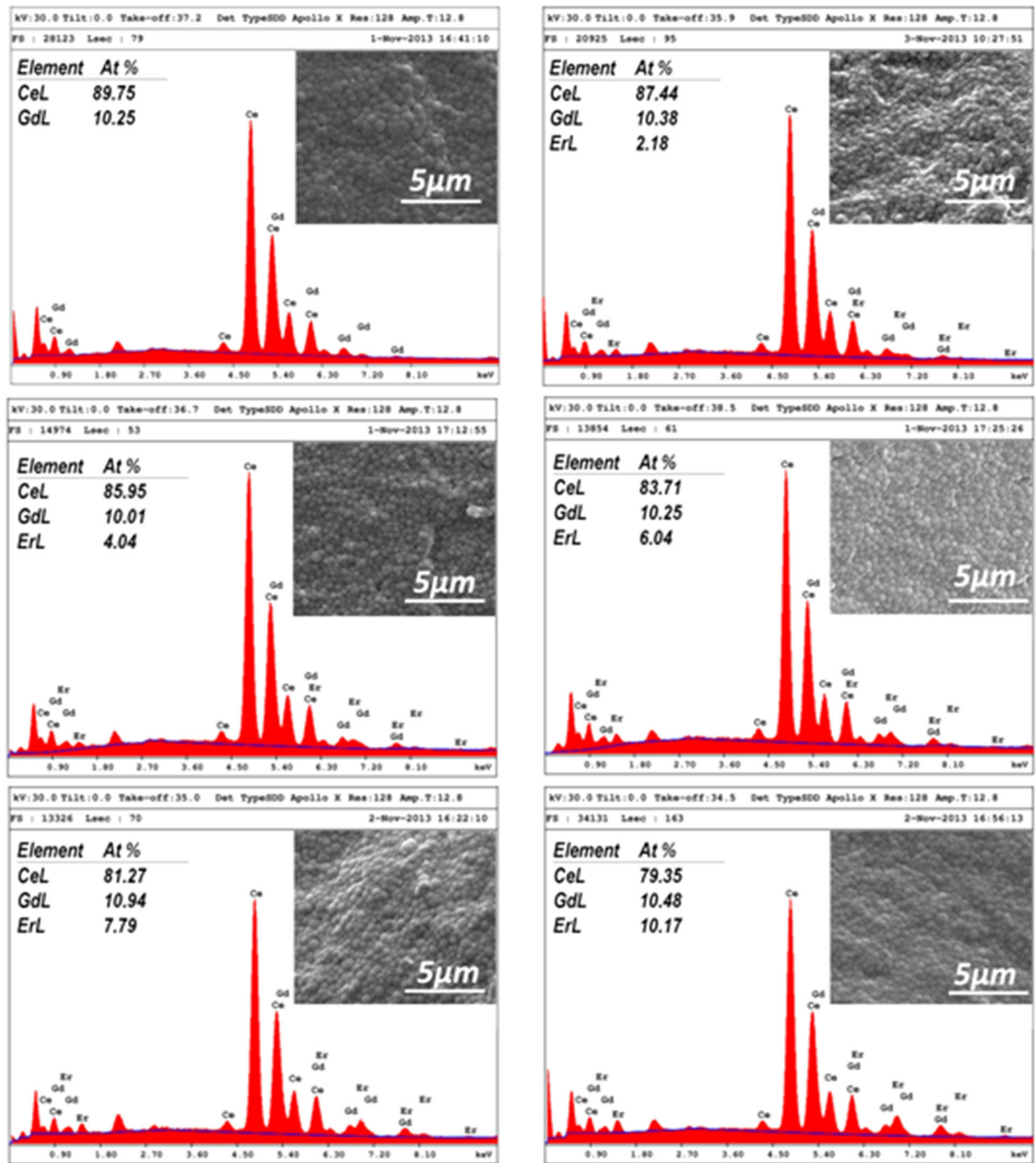
Fig. 8—EDS analysis of EGDC samples.

value of 2EGDC and 8EGDC samples at 573 K (300 °C). In order to see the lattice and grain boundary conductivity behavior, Figure 10(b) is plotted. As described, the high frequency arcs (low resistance region semicircle) are associated with the grain interior (lattice) resistance (R_{Gi}) and the second, low frequency arcs related with the grain boundary resistance (R_{Gb}). As can be seen in Figure 10(b) in detail, with the increasing Er dopant, only 2EGDC sample showed little lattice conductivity increment. Incorporation of 2 mol pct Er

into the lattice enhanced the oxygen ionic conductivity through improved oxygen vacancies. Over 2 mol pct Er, the grain interior resistance of the samples increased gradually. Actually, more incorporated dopant means more oxygen vacancies. However, in this study, lattice parameters decreased with the increasing dopant amount (pct Er). Thus, the migration of the oxygen ions into the lattice is likely to be hindered due to the shrinkage of the lattice. Therefore, the sample doped with 10 mol pct Er showed the lowest grain interior
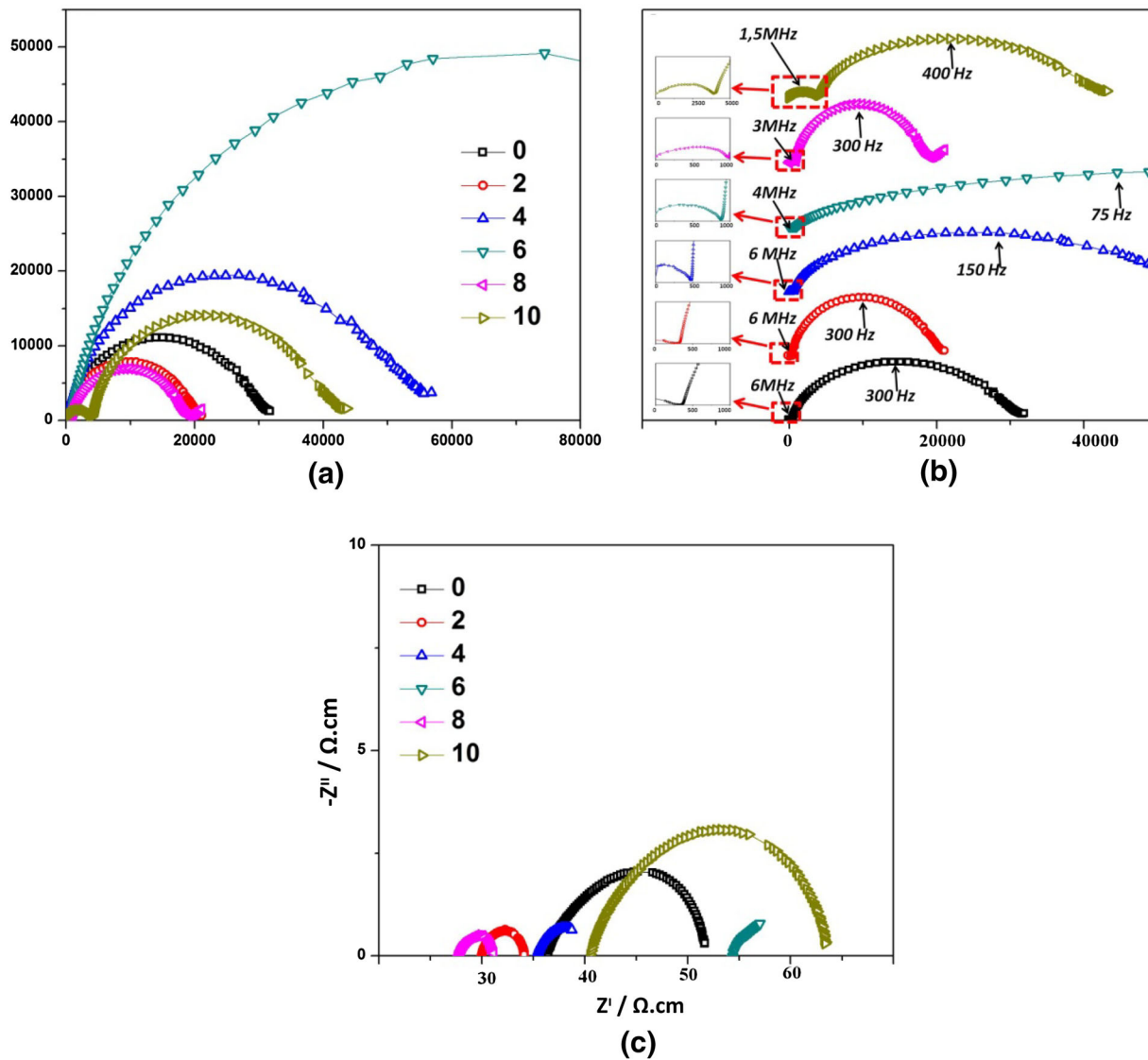
Fig. 9—SEM–EDS map analyses for 2EGDC sample.

Fig. 10—Complex impedance spectra plots of 0,0, 0.02, 0.04, 0.06, 0.08, and 0.10 mol. Pct Er-doped GDC pellets sintered at 1673 K (1400 °C), and measured (a, b) at 573 K (300 °C) and (c) at 1073 K (800 °C) in air (Color figure online).

ionic conductivity. It is understood from the impedance curves in Figure 10(b) that grain boundary conductivity (σ_{Gb}) effect is more dominant on the overall/total conductivity (σ_T) value of the GDC ceramics. R_{Gi}/R_T ratio is 1 pct for the GDC samples without Er; However, R_{Gi}/R_T ratio increased to 10 pct when GDC samples were doped with 8 mol pct Er. So, the grain

boundary properties have more important effect over the performance of the samples.

Figure 10(c) shows the high-temperature impedance curves. At these temperatures, the grain interior and grain boundary resistances become frequency independent, and the first intercept on Z′ shows the total resistance. As can be seen, the little differences on the
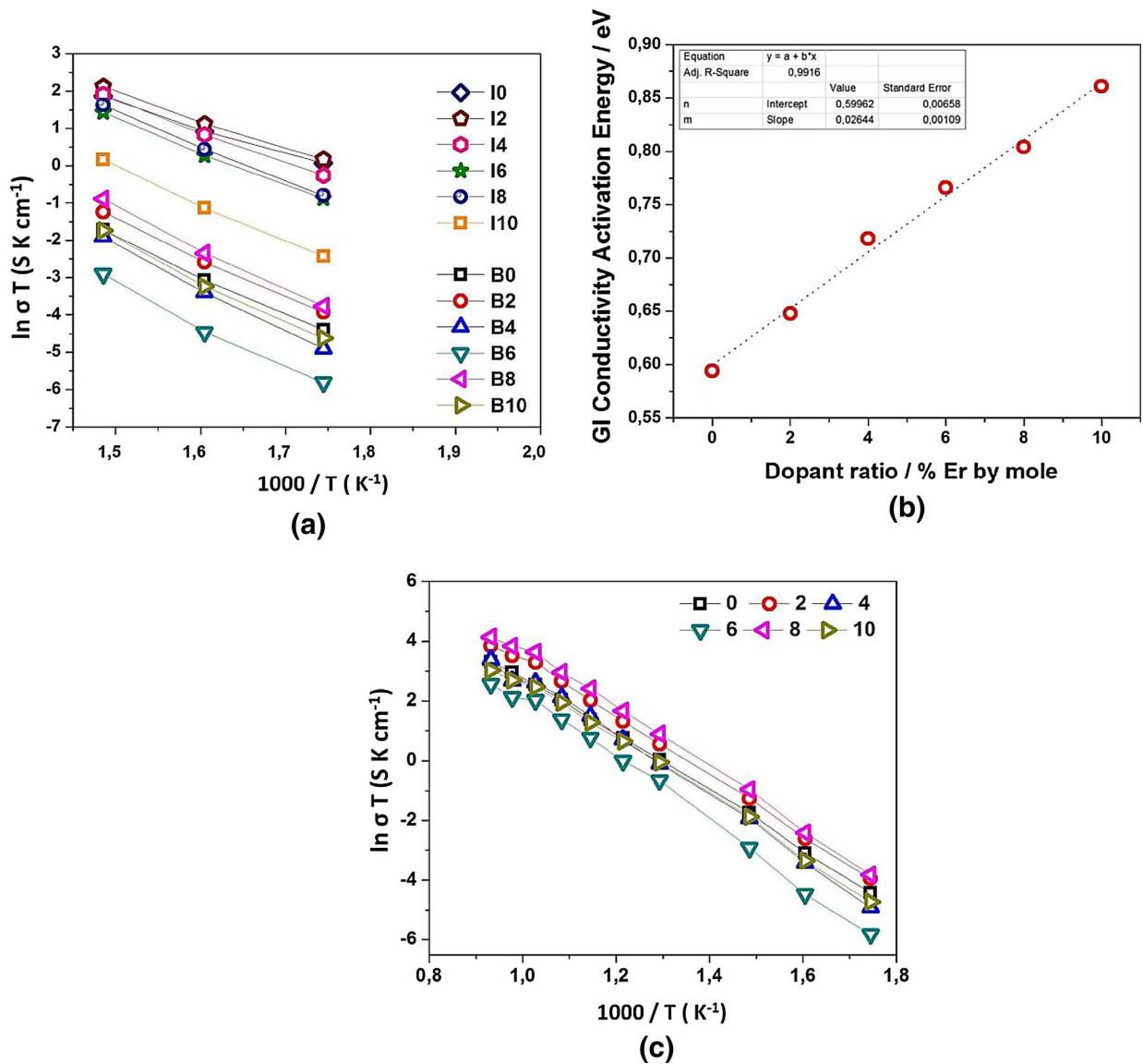
Fig. 11—Arrhenius plots of EGDC samples: (*a*) low temperature region grain interior (I0-10) and grain boundary (B0-10), (*b*) Grain Interior (GI) conductivity activation energy-pct Er relation, and (*c*) Arrhenius curves for samples for overall conductivity (Color figure online).

2EGDC and 8EGDC samples at 573 K (300 °C) become more clear and 8EGDC sample showed the best ionic conductivity at 1073 K (800 °C). Another remarkable difference is observed for the 4EGDC sample. At 573 K (300 °C), this sample showed lower conductivity than GDC, but at this temperature, 4EGDC also exhibited better performance than GDC sample. At 1073 K (800 °C), the ionic conductivity of the materials shows conductivity with the order of 8EGDC > 2EGDC > 4EGDC > GDC > 10EGDC > 6EGDC. For Er-free GDC sample, the ionic conductivity was calculated as 2.94×10^{-2} S cm^{-1} at 1073 K (800 °C). This value is compatible with and also higher than the results found in some other works in the literature. For example, Öksüzömer *et al.*[31] measured the ionic conductivity value as 2.29×10^{-2} S cm^{-1} at

1073 K (800 °C) for the GDC sample which was prepared by the polyol method while the calcination and sintering regimes were the same. This results show that CT method is a promising technique for the preparation of SOFC electrolyte materials. The ionic conductivity value of 8EGDC ($Ce_{0.82}Gd_{0.1}Er_{0.08}O_{1.91}$) was calculated as 3.57×10^{-2} S cm^{-1} at 1073 K (800 °C) which is 21 pct higher than that of Er-free GDC.

E_a values were calculated from the equation

$$\ln(\sigma \cdot T) = \ln(\sigma_o) - E_a/kT,$$

where $\ln(\sigma_o)$ is the intercept, E_a/k is the slope of the curve. $k = 8.61 \times 10^{-5}$ eV K^{-1}. A plot of $\ln(\sigma \cdot T)$ *vs* $1000/T$ should give a straight line where the slope of this

line is $-E_a/k$ if the activation energy E_a is independent of temperature.

Figure 11(a) shows the low temperature region grain boundary and grain interior Arrhenius lines. As can be seen, the I-series are ordered with the grain interior conductivity ranking, while the B-series are ordered not only with grain boundary but also total conductivity ranking, since the dominant effect for all samples is the grain boundary resistance. The slope of the curves in Figure 11(a) represents activation energy of grain boundary and grain interior conductivity. The grain interior activation energies of the samples were 0.594, 0.648, 0.718, 0.766, 0.804, and 0.861 eV for 0 to 10 EGDC, respectively. The grain interior (GI) conductivity activation energy *vs* pct Er ratio is given in Figure 11(b). It is seen that the GI activation energy changes linearly with the Er ratio with a high correlation factor, $R^2 = 0.991$. This behavior may also be an evidence for good incorporation of Er into Ce lattice which can be seen from the lattice parameter–Er ratio graph given in Figure 5. On the other hand, the same behavior was not observed with the grain boundary (GB) activation energy. The GB activation energy values are 0.89 to 0.96 eV without any trend with Er ratio. The GB activation energy range was so narrow, and it is not possible to infer any result with the Er ratio. On the other hand, the calculations showed that the highest σ_0 frequency factor was for the 8EGDC sample, and the lowest was for the 6EGDC sample like the conductivity values. This presents that, although activation energy values are effective on the lattice properties, it has a minimal effect on the grain boundary properties. Frequency factor is more dominant on the grain boundary properties than the activation energy. The overall activation energies of these compositions calculated from the slope of Arrhenius plot of total conductivity are in the range of 0.885 to 1.00 eV (LT), 0.45 to 0.69 eV (HT), respectively, which are consistent with the previously reported studies.[4,6,36]

The diversion in the Arrhenius plot of doped ceria electrolyte indicates a change in the mechanism for conduction changes at that particular temperature which can be taken as the transition temperature.[28] According to the Arrhenius plots of all samples in Figure 11(c), there are two parts: LT (low temperature) and HT (high temperature) regimes where the linearity of the plots changes; and thus, the activation energy of the bulk, grain, and overall conductivity changes with the increasing temperature. Oxygen ionic conductivity in RE-doped ceria can be given by the following equations:

$$\text{At low temperatures } \sigma = \frac{\sigma_0}{T} e^{-\frac{(\Delta H_m + \Delta H_a)}{kT}}, \qquad [3]$$

$$\text{At high temperatures } \sigma = \frac{\sigma_0}{T} e^{-\frac{(\Delta H_m)}{kT}}, \qquad [4]$$

where ΔH_m is the migration enthalpy of the oxygen ions, and ΔH_a is the association enthalpy of the dopant ion with the oxygen vacancies. Hence, the activation energy for conduction becomes the sum of the activation energy for migration and association ($E = E_m + E_a$). In general, it was suggested that at higher temperatures, the dopant-oxygen vacancy complex dissociates completely to free dopant cations and oxygen vacancy. The concentration of oxygen vacancy is independent of temperature and equivalent to the total concentration of dopant cations. Therefore, the migration enthalpy can be calculated from the slope of Arrhenius plots in the higher temperature regime. The association enthalpy can be calculated from the differences of the slopes at higher and lower temperature regimes.[45,46]

This study indicated that the impedance curve of the 2 mol pct Er-doped GDC ceramics showed the best GI conductivity, and 8 mol pct Er-doped GDC ceramics exhibited the best GB conductivity and so the best O_2-ionic conductivity value.

IV. CONCLUSIONS

For the first time, co-doped ceria samples $Ce_{0.9-x}Gd_{0.1}Er_xO_{1.9-x/2}$ ($x = 0.0, 0.02, 0.04, 0.06, 0.08, 0.1$) were successfully synthesized using the CT method. The CT method is a rapid and an economic process compared to the other synthesizing methods. Moreover, CT method enables to obtain smaller crystallite sizes (10.6 nm) at relatively low calcination temperatures. The XRD patterns of the samples prepared with the CT method exhibited the fluorite structure of CeO_2. Furthermore, the effect of concentration of Er on the properties of GDC was thoroughly studied. After sintering, the Er and Gd co-doped ceria pellets achieved over 95 pct of the theoretical density at 1673 K (at 1400 °C).

According to the EIS results, the ionic conductivity value of 8EGDC was calculated as 3.57×10^{-2} S cm^{-1} which is 21 pct higher than that of Er-free GDC. Due to the highest ionic conductivity, 8EGDC materials can be used as electrolytes for IT-SOFC applications instead of GDC. On the other hand, especially grain boundary behavior of Er-doped GDC must be investigated further in detail.

This paper discusses the detailed conductivity results related to the electrolyte materials that were synthesized using the CT method. Phase purity, stability, and RD are important factors for obtaining high-performance electrolytes for SOFCs. Therefore, CT method could be shown as a promising way to prepare of Er and Gd co-doped ceria-based electrolyte materials for SOFC economically. There are limited studies in the literature about the Er-RE materials co-doped ceria-based electrolyte materials for IT-SOFC. Additional studies will be performed to improve the ionic conductivity properties of the Er-rare earth materials co-doped ceria-based electrolytes.

REFERENCES

1. J.P.P. Huijsmans, F.P.F. van Berkel, and G.M. Christie: *J. Power Sources*, 1998, vol. 71, pp. 107–10.
2. H. Yoshida, K. Miura, T. Fukui, S. Ohara, and T. Inagaki: *J. Power Sources*, 2002, vol. 106, pp. 136–41.
3. X. Guan, H. Zhou, Y. Wang, and J. Zhang: *J. Alloys Compd.*, 2008, vol. 464, pp. 310–16.
4. S. Kuharuangrong: *J. Power Sources*, 2007, vol. 171, pp. 506–10.
5. D.H. Prasad, J.W. Son, B.K. Kim, H.W. Lee, and J.H. Lee: *J. Eur. Ceram. Soc.*, 2008, vol. 28, pp. 3107–12.
6. L.D. Jadhav, S.H. Pawar, and M.G. Chourashiya: *Bull. Mater. Sci.*, 2007, vol. 30, pp. 97–100.
7. S. Wang, T. Kobayashi, M. Dokiya, and T. Hashimoto: *J. Electrochem. Soc.*, 2000, vol. 147, pp. 3606–09.
8. M. Jamshidijam, R.V. Mangalaraja, A. Akbari-Fakhrabadi, S. Ananthakumar, and S.H. Chan: *Powder Technol.*, 2014, vol. 253, pp. 304–10.
9. F. Wang, S. Chen, Q. Wang, S. Yu, and S. Cheng: *Catal. Today*, 2004, vol. 97, pp. 189–94.
10. F.Y. Wang, S.Y. Chen, and S. Cheng: *Electrochem. Commun.*, 2004, vol. 6, pp. 743–46.
11. S. Lubke and H.D. Wiemhofer: *Solid State Ionics*, 1999, vol. 117, pp. 229–43.
12. X.Q. Sha, Z. Lu, X.Q. Huang, J.P. Miao, and L. Jia: *J. Alloys Compd.*, 2006, vol. 424, pp. 315–21.
13. T. Mori, J. Drennan, J.H. Lee, J.G. Li, and T. Ikegami: *Solid State Ionics*, 2002, vols. 154–155, pp. 461–66.
14. H. Yoshida, H. Deguchi, K. Miura, and M. Horiuchi: *Solid State Ionics*, 2001, vol. 140, pp. 191–99.
15. G.S. Wu, T. Xie, X.Y. Yuan, B.C. Cheng, and L.D. Zhang: *Mater. Res. Bull.*, 2004, vol. 39, pp. 1023–28.
16. M. Hirano and E. Kato: *J. Am. Ceram. Soc.*, 1996, vol. 79, pp. 777–80.
17. Y.C. Zhou and M.N. Rahman: *J. Mater. Res.*, 1993, vol. 8, pp. 1680–86.
18. N. Uekewa, M. Ueta, Y.J. Wu, and K. Kakewa: *Chem. Lett.*, 2002, vol. 8, p. 854.
19. H.I. Chen and H.Y. Chang: *Colloids Surf. A*, 2004, vol. 242, pp. 61–69.
20. C.R. Xia and M.L. Liu: *Solid State Ionics*, 2002, vol. 423, pp. 152–53.
21. M.M.A. Sekar, S.S. Manoharan, and K.C. Patil: *J. Mater. Sci. Lett.*, 1990, vol. 9, pp. 1205–06.
22. J. Chandradass, B. Nam, and K.H. Kim: *Colloids Surf. A*, 2009, vol. 348, pp. 130–36.
23. R.A. Rocha and E.N.S. Muccillo: *Mater. Res. Bull.*, 2003, vol. 38, pp. 1979–86.
24. B. Matovic, Z. Dohcevic-Mitrovic, M. Radovic, Z. Brankovic, G. Brankovic, S. Boskovic, and Z.V. Popovic: *J. Power Sources*, 2009, vol. 193, pp. 146–49.
25. A.N. Shigapov, G.W. Graham, R.W. McCabe, Jr, and H.K. Plummer: *Appl. Catal. A*, 2001, vol. 210, pp. 287–300.
26. K. Langfeld, R. Marschner, B. Frank, and R. Schomaker: *ChemCatChem*, 2011, vol. 3, pp. 1354–58.
27. B. Uslu, A. Aytimur, M.K. Ozturk, and S. Kocyigit: *Ceram. Int.*, 2012, vol. 38, pp. 4943–51.
28. S. Zha, C. Xia, and G. Meng: *J. Power Sources*, 2003, vol. 115, pp. 44–48.
29. V. Sarıboğa, H. Özdemir, and M.A.F. Öksüzömer: *J. Eur. Ceram. Soc.*, 2013, vol. 33, pp. 1435–46.
30. R.O. Fuentes and R.T. Baker: *J. Power Sources*, 2009, vol. 86, pp. 268–77.
31. M.A.F. Öksüzömer, G. Dönmez, V. Saribooğa, and T.G. Altınçekiç: *Ceram. Int.*, 2013, vol. 39, pp. 7305–15.
32. J. Li, T. Ikegami, and T. Mori: *Acta Mater.*, 2004, vol. 52, pp. 2221–28.
33. X. Guan, H. Zhou, Z. Liu, Y. Wang, and J. Zhang: *Mater. Res. Bull.*, 2008, vol. 43, pp. 1046–54.
34. S.J. Hong and A.V. Virkar: *J. Am. Ceram. Soc.*, 1995, vol. 78, pp. 433–39.
35. A. Gondolini, E. Mercadelli, A. Sanson, S. Albonetti, L. Doubova, and S. Boldrini: *Ceram. Int.*, 2011, vol. 37, pp. 1423–26.
36. C. Veranitisagul, A. Kaewvilai, W. Wattanathana, N. Koonsaeng, E. Traversa, and A. Laobuthee: *Ceram. Int.*, 2012, vol. 38, pp. 2403–09.
37. E. Barsoukov and J.R. MacDonald: *Impedance Spectroscopy Theory, Experiment, and Applications*, 2nd ed., Wiley, Hoboken, 2005.
38. J.E. Bauerle: *J. Phys. Chem. Solids*, 1969, vol. 30, pp. 2657–70.
39. J. Luo, R.J. Ball, and R. Stevens: *J. Mater. Sci.*, 2004, vol. 39, pp. 235–40.
40. J.G. Cheng, S.W. Zha, J. Huang, X.Q. Liu, and G.Y. Meng: *Mater. Chem. Phys.*, 2003, vol. 78, pp. 791–95.
41. M.G. Chourashiya, J.Y. Patil, S.H. Pawar, and L.D. Jadhav: *Mater. Chem. Phys.*, 2008, vol. 109, pp. 39–44.
42. S. Ramesh and C.V. Reddy: *Acta Phys. Pol. A*, 2009, vol. 115, pp. 909–13.
43. F.Y. Wang, B.Z. Wan, and S. Cheng: *J. Solid State Electrochem.*, 2005, vol. 9, pp. 168–73.
44. J. Kim and D. Lee: *Korean J. Chem. Eng.*, 2002, vol. 19, pp. 421–24.
45. J.A. Kilner and B.C.H. Steele:, in *Nonstoichiometric Oxides*, O.T. Sorensen, ed., Academic Press, New York, 1981, pp. 233–69.
46. S.C. Singhal and K. Kendall: *High Temperature Solid Oxide Fuel Cells: Fundamentals, Design, and Applications*, Elsevier, Oxford, 2003.